



HAL
open science

High-Permittivity Dielectric Probes for Ultra-High Field MR Microscopy at 17.2 T

Marine A.C. Moussu, Luisa Ciobanu, Elodie Georget, Stanislav B. Glybovski, Andrew G Webb, Stefan Enoch, Redha Abdeddaim

► **To cite this version:**

Marine A.C. Moussu, Luisa Ciobanu, Elodie Georget, Stanislav B. Glybovski, Andrew G Webb, et al.. High-Permittivity Dielectric Probes for Ultra-High Field MR Microscopy at 17.2 T. ISMRM 2020, Aug 2020, Sydney, Australia. hal-03164105

HAL Id: hal-03164105

<https://hal.science/hal-03164105>

Submitted on 9 Mar 2021

HAL is a multi-disciplinary open access archive for the deposit and dissemination of scientific research documents, whether they are published or not. The documents may come from teaching and research institutions in France or abroad, or from public or private research centers.

L'archive ouverte pluridisciplinaire **HAL**, est destinée au dépôt et à la diffusion de documents scientifiques de niveau recherche, publiés ou non, émanant des établissements d'enseignement et de recherche français ou étrangers, des laboratoires publics ou privés.

High-Permittivity Dielectric Probes for Ultra-High Field MR Microscopy at 17.2 T

M. A.C. Moussu^{1,2}, L. Ciobanu³, E. Georget¹, S. Glybovski⁴, A. G. Webb⁵, S. Enoch², R. Abdeddaim²

¹Multiwave Imaging, ²Aix-Marseille Univ., CNRS, Centrale Marseille, Institut Fresnel, ³DRF/Joliot/Neurospin/UNIRS, ⁴ITMO Univ., ⁵Leiden Univ. Medical Center

Synopsis

We propose a theoretical model predicting the Signal-to-Noise Ratio (SNR) of dielectric antennas for Magnetic Resonance Imaging. The SNR is estimated with a semi-analytical approach describing the first transverse electric mode of a high-permittivity ring resonator. When the ring is properly excited with a feeding loop, it induces a strong magnetic field in the sample while dielectric losses are limited due to low electric field intensity in this region. The proposed model is validated with numerical simulations regarding microscopy applications and its prediction confirmed experimentally at 17.2 T.

Summary of main findings

An alternative design of MR microscopy probes, based on dielectric ring resonators, is studied. A theoretical model for the achievable SNR is proposed and a prototype is built. It enables, at 17.2 T, a two-fold SNR enhancement compared to the conventional solenoid, as predicted by the model.

Introduction

Magnetic Resonance Microscopy (MRM) aims at imaging small samples with very high spatial resolution ($\ll 100 \mu\text{m}$) using B_0 field strengths between 7T and 22T¹. At such fields, the conventional RF coil is the solenoid. However, for lossy biological samples, its ultimate Signal-to-Noise Ratio (SNR) is intrinsically limited by the significant electric field within the sample. Dielectric resonators are an alternative probe design to tackle this issue^{3,4}: high-permittivity rings support eigenmodes whose frequency characteristics rely on the resonator dimensions and the material properties^{5,6}. The first transverse electric mode ($TE_{01\delta}$) produces a strong B_1 excitation field (Fig. 1), and a low E-field. Here we present a semi-analytical model (SAM) to design dielectric ring probes with high SNR⁷. This model is validated with numerical simulations and experimentally tested for MRM at 17.2 T⁸.

Methods

The noise is dominated by losses in the dielectric ring (volume V_{ring} , outer and inner radii r_d and r_h , height L , permittivity $\epsilon = \epsilon_0(\epsilon_r - i\omega \tan \delta)$) and in the sample (volume V_{samp} , radius r_h , height L , electrical conductivity σ_{samp}). The SNR is proportional to the SNR factor (Eq. 1) with $H_{\text{samp}}(0)$ the H-field amplitude in the sample, and P_{loss} (Eq. 2)⁹ the total dielectric losses.

$$\text{(Eq. 1)} \quad u_{\text{SNR}} = H_{\text{samp}}(0) / \sqrt{P_{\text{loss}}}$$

$$\text{(Eq. 2)} \quad P_{\text{loss}} = \frac{1}{2} \omega \epsilon'' \int_{V_{\text{ring}}} |\mathbf{E}|^2 dv + \frac{1}{2} \sigma_{\text{samp}} \int_{V_{\text{samp}}} |\mathbf{E}|^2 dv$$

The $TE_{01\delta}$ mode field is described by Bessel and Hankel functions in cylindrical coordinates (ρ, θ, y) . As this mode has a cylindrical symmetry, H_y , H_ρ and E_θ are the only nonzero components¹⁰. Expressing H_y , as in Eqs. 3-4 with α_Ω and β_Ω the wavenumbers in region Ω , enables to derive the other components^{11,12}.

$$\text{(Eq. 3)} \quad H_{y,\text{samp}}(\rho, y) \propto J_0(\alpha_{\text{samp}}\rho) \cos(\beta_{\text{samp}}y)$$

$$\text{(Eq. 4)} \quad H_{y,\text{ring}}(\rho, y) \propto \left[H_0^{(1)}(\alpha_{\text{ring}}\rho) + \xi H_0^{(2)}(\alpha_{\text{ring}}\rho) \right] \cos(\beta_{\text{ring}}y)$$

The E-field, derived from the spatial derivative of H_y , is proportional to the H-field amplitude. In Eq. 3, this amplitude is $H_{\text{samp}}(0)$. To analytically express dielectric losses, the probe EM field is simplified to that of the corresponding disk: $\mathbf{E}(\vec{r})|_{\text{ring}} = \mathbf{E}(\vec{r})|_{\text{disk}}$, $\mathbf{E}(\vec{r})|_{\text{sample}} = \tau \mathbf{E}(\vec{r})|_{\text{disk}}$ and $\mathbf{E}(\vec{r})|_{\text{disk}} \propto J_1(\alpha_{\text{disk}} \rho) \vec{e}_\theta$. τ reflects the amplitude decrease from permittivity contrast between the sample and the ring. Eq. 1 becomes Eq. 5 with $P_{\text{loss},\text{norm}}^i = P_{\text{loss}}^i / |H_{\text{disk}}(0)|^2$.

$$\text{(Eq. 5)} \quad u_{\text{SNR}}^{\text{DR}} = \tau / \sqrt{P_{\text{loss},\text{norm}}^{\text{ring}} + \tau^2 P_{\text{loss},\text{norm}}^{\text{sample}}}$$

A Frequency Domain Solver (CST Microwave Studio) was used to evaluate the EM field excited in the dielectric probe by a 1 cm diameter non-resonant loop. In a “combined method”, the SNR factor is computed with Eq. 5 applied to the field exported from numerical simulations run in the CST Eigenmode Solver.

The experimental resonator was built with a ferroelectric ceramic⁸ with the following parameters at 730 MHz (Larmor frequency at 17.2 T): $r_d = 9 \text{ mm}$, $r_h = 2.8 \text{ mm}$, $L = 10 \text{ mm}$, $\epsilon_r = 536$, $\tan \delta = 8 \times 10^{-4}$. The phantom used was a tube of diameter 4.5 mm and length 12 mm filled with a solution of permittivity $\epsilon_{r,\text{test}} = 50$ and conductivity $\sigma_{\text{tes}} = 1 \text{ S/m}$. The corresponding optimal solenoid has 4 turns, 7 mm diameter, 12 mm length and is made with 1.5 diameter copper wire². Its SNR factor $u_{\text{SNR}}^{\text{sol}}$ can be found in the literature². MRI acquisitions were performed on a preclinical device (Bruker BioSpin, Ettlingen, Germany) equipped with a triaxial gradient system of maximum strength 1 T/m. The biological sample studied was a chemically fixed rat spinal cord. MR acquisitions were performed with sequences described in Fig. 2.

Results

The SAM was used to estimate the SNR gain $u_{\text{SNR}}^{\text{DR}} / u_{\text{SNR}}^{\text{sol}}$, plotted in Fig. 3 for the phantom as a function of the dielectric properties. For each permittivity, r_d was adapted to adjust the $\text{TE}_{01\delta}$ mode to the Larmor frequency. When $\tan \delta \leq 2.10^{-3}$ and $\epsilon_r \geq 220$, the semi-analytical method predicts a higher SNR with the dielectric probe than with the optimal solenoid. From this dependency, the prototype properties were selected, resulting in a theoretical SNR gain of 2.5. The prototype SNR factor was computed using the SAM and compared to numerical simulations and a combined method as shown in Fig. 4. The sample permittivities were 50 and 81 and its conductivity was varied from 0 to 2.5 S/m. The relative error between the SAM and the commercial software was always below 8%⁷. Finally, experiments performed on the test solution resulted in a measured SNR gain of 2.2 (versus 2.5 theoretically), as obtained with numerical simulations. Fig. 5 demonstrates that the ceramic probe performs better than the optimal solenoid when imaging the biological sample, with an SNR gain of 1.45.

Discussion

The SAM estimates the SNR factor with an error lower than 8% over a large range of electromagnetic properties. The SNR gain estimation was validated in one case, in which the predicted value was within 15% of the experimentally measured value.

Conclusion

This study focused on the modelling of dielectric ring probes in which the first TE mode is excited to generate the B_1 field used in MR acquisitions. The semi-analytical model predicts the performance of such probes with a good accuracy and can be used as a design guideline. Our current and future work

includes the extension of dielectric probes modelling to clinical applications. This includes resonators with human scale dimensions, as well as the study of higher resonant modes (like HEM modes).

Acknowledgements

This project received funding from the European Union's Horizon 2020 Research and Innovation programme (grant No 736937) and from an ERC Advanced Grant (NOMA-MRI 670629). S.G. acknowledges the support by the President of the Russian Federation (MK-3620.2019.8)

References

1. Ciobanu, L. (2017). *Microscopic Magnetic Resonance Imaging: A Practical Perspective*. Pan Stanford.
2. Minard, K. R., & Wind, R. A. (2001). Solenoidal microcoil design—Part II: Optimizing winding parameters for maximum signal-to-noise performance. *Concepts in Magnetic Resonance*, 13(3), 190-210.
3. Haines, K., Neuberger, T., Lanagan, M., Semouchkina, E., & Webb, A. G. (2009). High Q calcium titanate cylindrical dielectric resonators for magnetic resonance microimaging. *Journal of Magnetic Resonance*, 200(2), 349-353.
4. Neuberger, T., Tyagi, V., Semouchkina, E., Lanagan, M., Baker, A., Haines, K., & Webb, A. G. (2008). Design of a ceramic dielectric resonator for NMR microimaging at 14.1 tesla. *Concepts in Magnetic Resonance Part B: Magnetic Resonance Engineering: An Educational Journal*, 33(2), 109-114.
5. Mongia, R. K., & Bhartia, P. (1994). Dielectric resonator antennas—A review and general design relations for resonant frequency and bandwidth. *International Journal of Microwave and Millimeter-Wave Computer-Aided Engineering*, 4(3), 230-247.
6. Kajfez, D., & Guillon, P. (1998). *Dielectric resonators* (p. 547). Atlanta: Noble Publishing Corporation.
7. Moussu, M. A.C., Abdeddaim, R., Dubois, M., Georget, E., Webb, A. G., Nenasheva, E., Belov, P., Glybovski, S., Ciobanu, L., & Enoch, S. (2019). A Semi-Analytical Model Of High Permittivity Dielectric Ring Resonators for Magnetic Resonance Imaging. Under review.
8. Moussu, M. A., Ciobanu, L., Kurdjumov, S., Nenasheva, E., Djemai, B., Dubois, M., ... & Glybovski, S. (2019). Systematic Analysis of the Improvements in Magnetic Resonance Microscopy with Ferroelectric Composite Ceramics. *Advanced Materials*, 1900912.
9. Petit, R. (1989). *Ondes électromagnétiques en radioélectricité et en optique* (Vol. 2). Paris: Masson.
10. Pozar, D. M. (2009). *Microwave engineering*. John Wiley & Sons.
11. Zhang, K., Li, D., Chang, K., Zhang, K., & Li, D. (1998). *Electromagnetic theory for microwaves and optoelectronics* (pp. 274-283). Berlin: Springer.
12. Sheen, J. (2008). A dielectric resonator method of measuring dielectric properties of low loss materials in the microwave region. *Measurement Science and Technology*, 19(5), 055701.

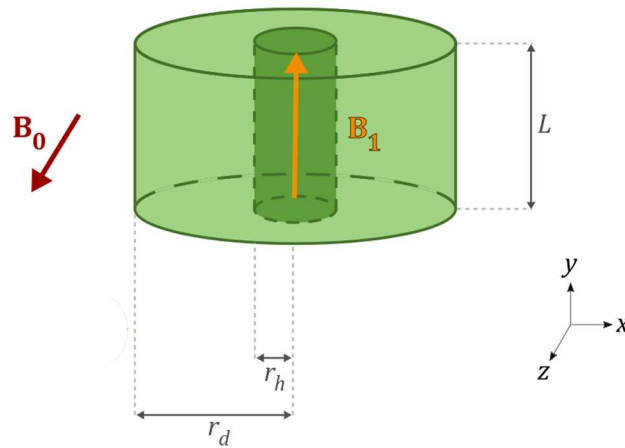


Fig. 1 – Dielectric probe based on its TE_{01δ} mode: notations and field directions.

MR ACQUISITION	SNR ESTIMATION	RAT SPINAL CORD SAMPLE
SEQUENCE TYPE	Gradient Echo	FLASH
TR/TE (MS)	1000/6	300/12
FLIP ANGLE (°)	30	30
FIELD OF VIEW (MM X MM)	10 x 10	4.5 x 4.5 x 2
SLICE THICKNESS (MM)	0.5	N.A.
MATRIX SIZE	128 x 128	182 x 182 x 40
RESOLUTION	0.078 mm x 0.078 mm	25 μm x 25 μm x 25 μm
ACQUISITION TIME	2 min 8 s	36 min

Fig. 2 – Sequence parameters for the two types of MR acquisitions

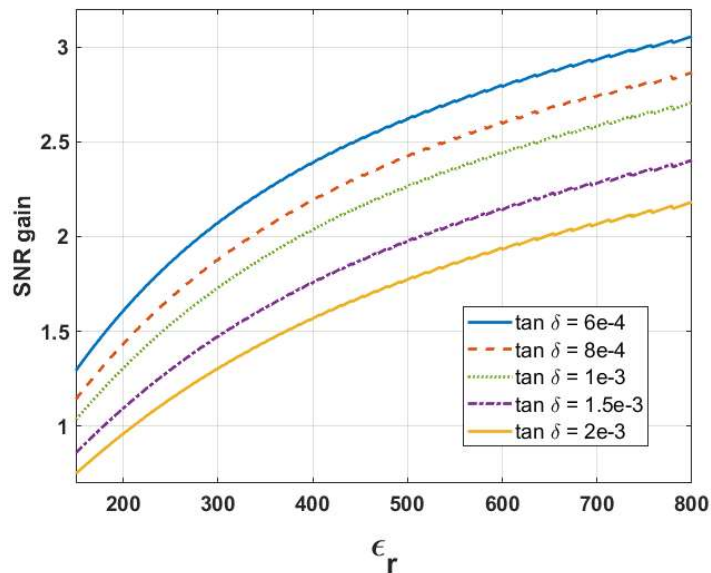


Fig. 3 – SNR gain for the phantom as a function of the ring dielectric material permittivity (ϵ_r) and for several loss tangent values ($\tan \delta$).

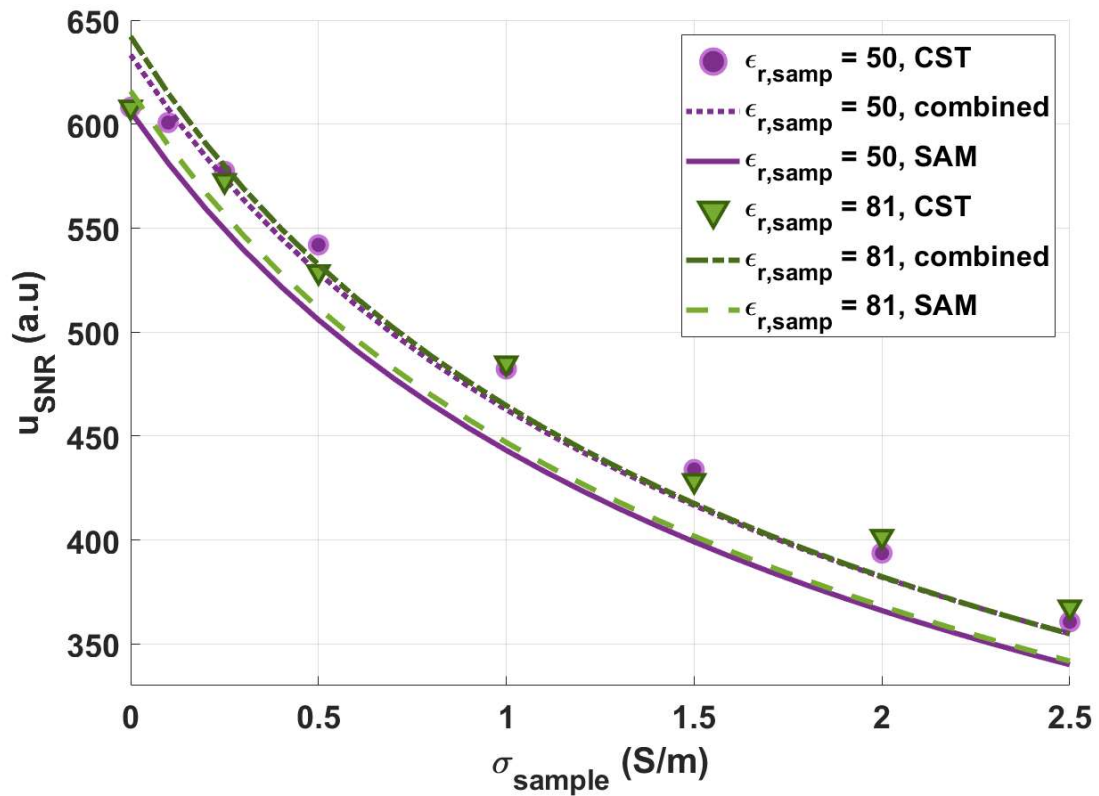


Fig. 4 – Simulated SNR factor of a ring resonator with same properties as the experimental probe^{8,7} for two realistic sample properties. The graph shows a comparison between numerical simulations (Frequency Domain Solver), the SAM, and the combined method. The maximum relative error between CST and SAM is 8%.

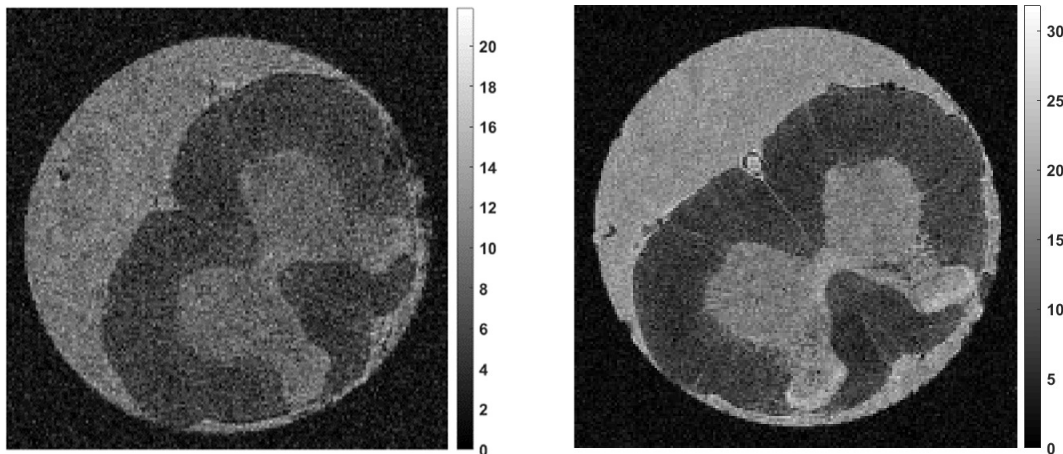


Fig. 5 – Ex vivo rat spinal cord acquisition : SNR map in one axial plane. Resolution: $(25\mu\text{m})^3$. Left: solenoid, max SNR = 21.9. Right: ceramic, max SNR = 31.9.